



Cite this: *CrystEngComm*, 2025, 27, 302

Received 31st October 2024,
Accepted 10th December 2024

DOI: 10.1039/d4ce01108b

rsc.li/crystengcomm

Rapid co-reduction synthesis of ultrafine multi-principal element alloy nanocatalysts for efficient hydrogen evolution†

Yongjun Jiang, Yuankai Zhu, Yanyan Jia* and Sheng Dai *

A rapid co-reduction strategy for the synthesis of ultrafine and composition-tunable multi-principal element alloy catalysts is proposed. This method necessitates only a 10-minute reaction time at 180 °C and features straightforward setups. The as-synthesized carbon-supported RuPtIrSnCu nanoparticles exhibit superior hydrogen evolution reaction performance in acidic media due to synergistic effects among their multiple components.

Multi-principal element alloys (MPEAs), containing three or more components in high concentrations, represent a novel class of materials with excellent properties and broad application potential.^{1–7} The synergistic interactions among the various elements in MPEAs yield entropy effects, diverse active sites, high stability, and corrosion resistance.^{8,9} When down to the nanoscale, MPEAs not only retain these advantages but also exhibit enhanced catalytic activity and stability due to their high surface area and quantum size effects, particularly in energy and catalysis applications.^{10,11}

However, synthesizing MPEA nanomaterials and fully controlling their components present considerable challenges. This is primarily due to difficulties in achieving a uniform mixture and distribution of multiple metal elements at the nanoscale, which arises from the variations in redox potentials among different metal elements. Significant efforts have been made to address this issue. To narrow the gap in redox potentials, researchers often employ extreme conditions for the preparation of MPEA nanoparticles. Notably, the carbothermal shock method stands out, where a carbon-supported mixture of metal salts is heated to approximately 2000 K within about 55 ms, followed by rapid cooling at a rate of 10^5 K s^{-1} .¹² In addition to this method, other synthesizing

approaches, including the laser ablation method,^{13,14} sputter deposition,¹⁵ and fast pyrolysis,¹⁶ are developed for the synthesis of MPEA nanoparticles. However, these methods frequently require expensive specialized equipment, extreme manufacturing conditions, and complex operational procedures. Moreover, such extreme environments can hinder precise control over the nanoparticle size and surface structure, both of which are critical for catalytic applications.^{17,18} Therefore, it is particularly important to develop a simple and mild preparation synthesis for MPEA nanoparticles.

Wet-chemical synthesis is an important approach for nanomaterial preparation, characterized by mild reaction conditions, simple equipment requirements, strong adaptability, and ease of manipulation, holding significant promise and research value in the field of nanomaterials and nanotechnology. Over the past decades, wet-chemical synthesis has advanced considerably, particularly in the controllable synthesis of highly dispersed binary and ternary component nanomaterials.^{19,20} Despite recent progress in the controllable preparation of MPEA nanoparticles using wet-chemical synthesis, significant challenges are still remaining.⁸ These challenges manifest primarily in two areas: (1) how can we narrow the redox potential gaps among different metal elements to facilitate the co-reduction of multiple components, thereby achieving uniform mixing within the nanoparticles? (2) How can we control the uniformity of nanoparticles without employing surface modifiers? Although surface modifiers can effectively regulate the nanoparticle morphology and uniformity,²¹ they often coordinate with metal elements, affecting their reduction rates. Additionally, the use of excessive amounts of surfactants can cover the active sites of catalysts, resulting in decreased catalytic activity.²²

Herein, we developed a rapid co-reduction strategy for synthesizing ultrafine, composition-tunable, and highly dispersive carbon black-supported MPEA nanoparticles. This strategy employs ethylene glycol as a strong reducing agent to co-reduce the uniformly mixed metal precursors at 180 °C,

Key Laboratory for Advanced Materials and Feringa Nobel Prize Scientist Joint Research Center, School of Chemistry & Molecular Engineering, East China University of Science and Technology, Shanghai 200237, P.R. China.

E-mail: jiaanyan@ecust.edu.cn, shengdai@ecust.edu.cn

† Electronic supplementary information (ESI) available. See DOI: <https://doi.org/10.1039/d4ce01108b>

enabling the preparation of MPEAs in just 10 minutes. The high viscosity of both the strong reducing agent (ethylene glycol) and the dispersion solvent (triethylene glycol for the metal precursors) facilitates the formation of extremely fine and uniform MPEA nanoparticles composed of any combination of the five elements (Pt, Ru, Ir, Sn, and Cu) even without the use of surfactants. In addition, electrochemical tests demonstrated that the as-synthesized MPEA nanoparticles exhibited enhanced hydrogen evolution reaction (HER) activity and stability compared to the commercial Pt/C catalysts. Particularly, RuPtIrSnCu/C displayed superior HER performance due to the synergistic effects among its multiple components. This innovation not only reduces the reliance on harmful chemicals but also significantly enhances synthesis efficiency, eliminating the need for complex or expensive auxiliary experimental equipment for the controlled production of high-quality MPEA nanomaterials.

Fig. 1 illustrates the synthesis process of alloy nanoparticles, which employs a rapid co-reduction strategy *via* an improved wet chemical synthesis method. Initially, solution A is prepared by adding metal precursors in equimolar proportions to 10 ml of triethylene glycol solution and subjecting the mixture to ultrasonic dissolution to obtain an evenly mixed metal precursor solution. Subsequently, solution B is formulated by ultrasonically dispersing the carbon black support in 100 ml of ethylene glycol solution, which is then heated to 180 °C and maintained at that temperature. Due to the strong reducibility of ethylene glycol, the uniformly mixed metal precursor solution can be rapidly reduced to metal alloy nanoparticles under high-temperature conditions. Once solution B reaches the desired temperature, solution A is added dropwise to ensure that each aliquot of solution A is quickly reduced upon addition. This process takes place over 10 minutes for the whole reaction. Subsequently, the reaction mixture is quickly cooled to room temperature using an ice water bath to halt the reduction reaction promptly. This rapid cooling helps prevent uneven particle formation and phase separation that can occur due to the gradual maturation of metal particles caused by slow changes in the time and temperature.

This synthesis method requires only conventional laboratory equipment and enables the controllable preparation of multi-component alloy nanoparticles within a

brief reaction time of 10 minutes, under mild and straightforward experimental conditions. Here, we synthesized RuPt/C, RuPtIr/C, RuPtIrSn/C, and RuPtIrSnCu/C alloy nanoparticles as examples. Importantly, this method does not involve any surfactants, resulting in clean surfaces for the prepared nanocatalysts. Combining all the above advantages, the proposed synthesis method offers significant benefits for the facile preparation of MPEA nanomaterials.

Inductively coupled plasma optical emission spectroscopy (ICP-OES) was first performed to confirm the multiple elemental composition of the as-synthesized MPEA nanoparticles. The results summarized in Table S1† demonstrate that the synthesized samples were composed of a diverse range of metal elements and the total metal loading in the alloy nanocatalysts was approximately 10%. Fig. 2a displays the XRD patterns of the as-prepared RuPt/C, RuPtIr/C, RuPtIrSn/C, and RuPtIrSnCu/C nanocatalysts. The XRD patterns of all samples reveal three prominent diffraction peaks centered at $2\theta = 25^\circ$, 41° , and 70° . Notably, the broad peak observed around 25° corresponds to the presence of the carbon support, while the latter two peaks represent the characteristic (111) and (220) planes of the face-centered cubic (FCC) phase, respectively.^{23,24} The XRD patterns of all samples exhibited these characteristic FCC peaks, indicating that the structure remained unaffected by changes in the elemental composition. Furthermore, with the incorporation of Ir and Sn, the peaks of RuPtIrSnCu/C and RuPtIrSn/C shifted towards lower angles, showing the existence of strong high-entropy effects.⁴ The significant broadening of the diffraction peaks of these alloy samples suggests that the size of the metal alloy particles is extremely small.

Moreover, aberration-corrected transmission electron microscopy (AC-TEM) was conducted for a detailed structure of the metal alloy particles. Fig. S1† presents the overviewing TEM images and particle size distributions of these MPEA nanocatalysts, illustrating high dispersion on the carbon support with uniform particle sizes with an average diameter of approximately 3.0 nm. Based on the high-resolution TEM (HRTEM) images coupled with their corresponding fast Fourier transform (FFT) patterns (Fig. 2b–e), the electron diffraction of RuPt/C, RuPtIr/C, RuPtIrSn/C, and RuPtIrSnCu/C can be indexed as the FCC structure. In addition, the lattice spacings of the FCC(111) plane in the as-synthesized particles

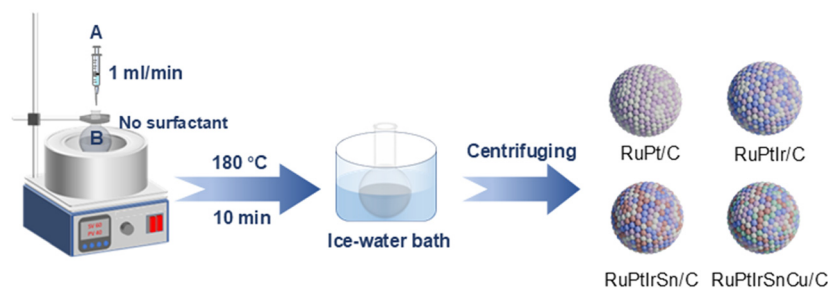


Fig. 1 Schematic of the rapid co-reduction synthesis of MPEA nanoparticles.

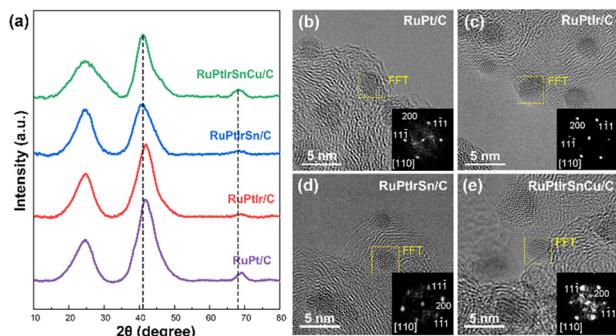


Fig. 2 (a) XRD patterns of the as-synthesized MPEA nanocatalysts. (b–e) HRTEM images and the corresponding FFT patterns (the insets) of RuPt/C, RuPtIr/C, RuPtIrSn/C, and RuPtIrSnCu/C alloy nanocatalysts.

are summarized in Table S2.† Due to the larger size of Sn atoms, the particles that contain Sn show increased lattice spacings, consistent with the trend in the XRD results. Fig. 3 represents the atomic-scale high-angle annular dark-field scanning transmission electron microscopy (HAADF-STEM) images and the corresponding energy-dispersive X-ray spectroscopy (EDS) elemental maps of RuPt/C, RuPtIr/C, RuPtIrSn/C, and RuPtIrSnCu/C, confirming their homogeneous elemental distributions within the particles. These results clearly illustrate the well-defined alloy structure of the as-prepared MPEA nanomaterials. More importantly, this co-reduction synthesis method was extended to prepare other alloy nanocatalysts containing Ru, Pt, Ir, Sn, and Cu.

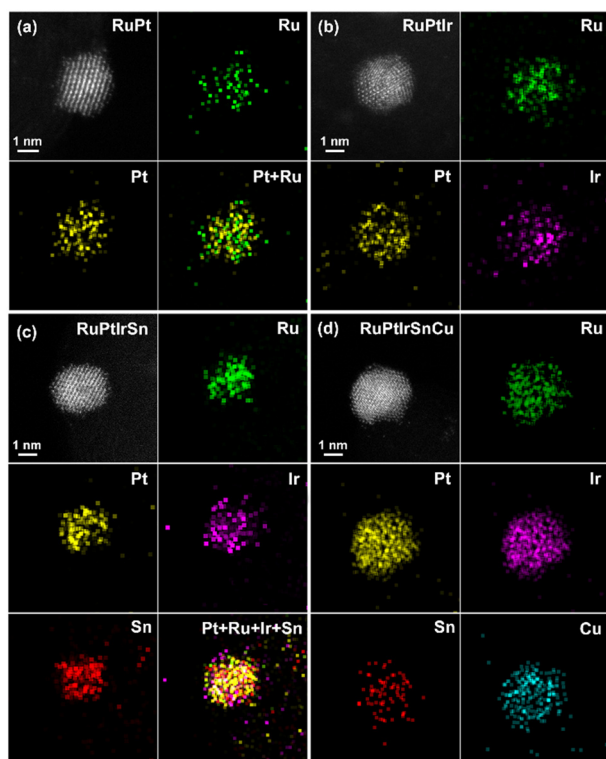


Fig. 3 Atomic-scale HAADF-STEM images and the corresponding EDS elemental maps of MPEA nanoparticles (a) RuPt, (b) RuPtIr, (c) RuPtIrSn, and (d) RuPtIrSnCu.

These alloy nanoparticles also exhibit uniform size and high dispersion (Fig. S2†). HRTEM images and their corresponding FFT patterns confirm their FCC structures (Fig. S3†), while the EDS elemental maps further confirm the homogeneous distribution of each element (Fig. S4†).

To verify the necessity of the rapid co-reduction strategy, a control experiment with an extended reaction time of one hour was conducted. The result reveals an inhomogeneous elemental distribution, showing an obvious segregation of Pt and Ir with a prolonged reaction time. Meanwhile, the size distribution became much wider due to agglomeration (Fig. S5†). Moreover, in comparison to other synthesis approaches for MPEA nanoparticles, as summarized in Table S3,† our rapid co-reduction strategy shows advantages in terms of convenience and efficiency.

The electrochemical hydrogen evolution reaction (HER) performance of these as-synthesized MPEA catalysts was then evaluated in an acid solution (0.5 M H₂SO₄). For comparison, the electrocatalytic activities of commercial Pt/C (20 wt%) were also tested as benchmarks under the same conditions. The linear sweep voltammetry (LSV) curves with an iR compensation in N₂-saturated 0.5 M H₂SO₄ at a scan rate of 5 mV s⁻¹ are shown in Fig. 4a. The potentials for the RuPt/C, RuPtIr/C, RuPtIrSn/C, and RuPtIrSnCu/C catalysts are lower than that of commercial Pt/C at the same current density, indicating that the HER activities of all MPEA nanocatalysts exceed that of the commercial Pt/C catalyst.

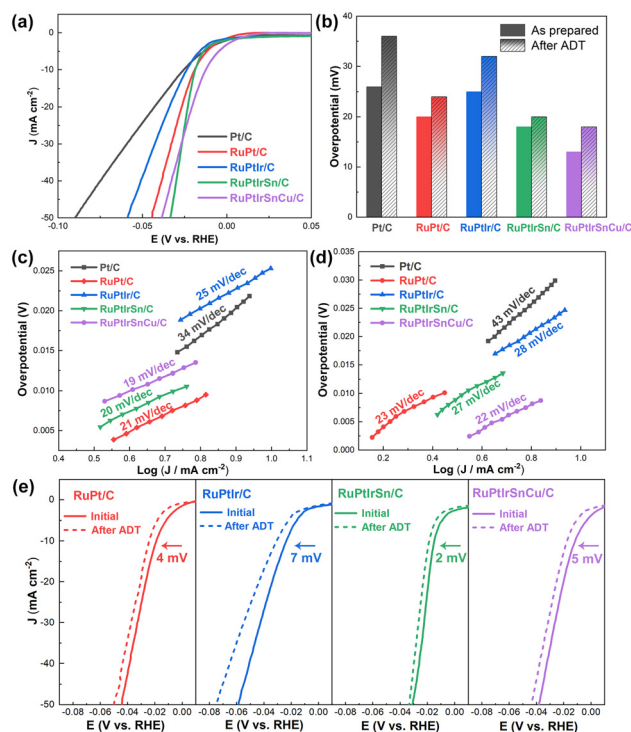


Fig. 4 Electrochemical evaluation of the as-prepared binary and MPEA catalysts. (a) LSV curves of commercial Pt/C and MPEA catalysts, (b–e) overpotentials at 10 mA cm⁻², Tafel plots and LSV curves of commercial Pt/C, RuPt/C, RuPtIr/C, RuPtIrSn/C, and RuPtIrSnCu/C nanocatalysts before and after 5000 cycles of the ADT in 0.5 M H₂SO₄.

In Fig. 4b, the overpotential values at 10 mA cm^{-2} reveal that RuPt/C exhibited an overpotential of 20 mV, smaller than that of Pt/C (26 mV). The overpotentials for RuPtIr/C, RuPtIrSn/C, and RuPtIrSnCu/C are 25 mV, 18 mV, and 13 mV, respectively, further demonstrating their improved HER performances. This trend indicates that the HER activity has been significantly enhanced with the increase in components within the MPEAs. In addition, Tafel slopes, plotted from the HER polarization curves, were used to explore the electrocatalytic mechanism of the HER (Fig. 4c). The Tafel slopes for RuPt/C, RuPtIr/C, RuPtIrSn/C, and RuPtIrSnCu/C are 21, 25, 20, and 19 mV dec^{-1} , respectively, all of which are lower than that for commercial Pt/C (34 mV dec^{-1}). This suggests that the HER kinetics are accelerated by the MPEA composition. The HER of these MPEA catalysts follow the Volmer–Tafel mechanism, similar to that of commercial Pt/C. It is widely recognized that the HER activities of catalysts are mainly determined by the adsorption energy of the intermediate H species.²⁵ Fig. S6† shows the normalized CV curves of those electrocatalysts in 0.5 M H_2SO_4 solution. All CV curves display the characteristic features of hydrogen adsorption and desorption peaks within the potential range of -0.2 V to 0.0 V . As the number of elemental components in the MPEA catalysts increases, the central potential of the H desorption peak first shifts to the left and then to the right, ultimately stabilizing around -0.11 V . This behavior indicates that a great number of components in the MPEAs effectively modulate the H adsorption and desorption. The optimized electronic structure of Pt sites, enhanced by the synergistic effect in the MPEAs, enables the Pt site to achieve optimum Pt–H binding, which might lead to a rapid H^+ adsorption and H_2 release process, ultimately accelerating the HER.²⁶ In addition, the addition of Sn and Ru can significantly lower the water dissociation energy barrier, facilitating the kinetics of the HER.²⁷ Therefore, the MPEA catalyst demonstrates improved catalytic activity compared to Pt/C, and RuPtIrSnCu/C exhibits the best HER activity.

The long-term durability of the as-prepared MPEA nanoparticles was assessed by the accelerated degradation test (ADT) in a 0.5 M H_2SO_4 solution. The changes of overpotentials, LSV curves, Tafel slopes, and CV curves are depicted in Fig. 4b–e and S6.† The LSV curves of RuPt/C, RuPtIr/C, RuPtIrSn/C, and RuPtIrSnCu/C measured before and after 5000 cycles of the ADT show smaller variations compared to that of commercial Pt/C in the acid electrolyte (Fig. 4e). Both the binary and MPEAs synthesized using the rapid co-reduction method exhibit excellent stability. The overpotentials of RuPt/C, RuPtIr/C, RuPtIrSn/C, and RuPtIrSnCu/C increased by only 4, 7, 2 and 5 mV, respectively, after 5000 cycles. After the long-term stability test, the Tafel slopes for the RuPt/C, RuPtIr/C, RuPtIrSn/C, and RuPtIrSnCu/C catalysts were found to be 23, 28, 27, and 22 mV dec^{-1} , respectively, showing negligible changes compared to their values before the ADT (Fig. 4c and d). In addition, the electrochemical performance of MPEA catalysts with other combinations of the five elements is summarized

in Fig. S7.† The overpotentials and Tafel slopes before and after the ADT of all MPEA catalysts in this work are summarized in Table S4.† It is evident that all MPEA nanoparticles synthesized using this co-reduction method exhibit excellent electrochemical stability compared to commercial Pt/C. Moreover, the high mixing entropy within the structure effectively mitigates the degradation and corrosion of the alloy, thereby enhancing its stability.²⁸

Overall, a comprehensive evaluation of both the activity and stability indicates that the RuPtIrSnCu/C catalyst exhibits the best HER performance, attributed to the synergistic effects among its multiple components and the high-entropy effect. Notably, these effects are amplified along with the increasing number of components.²⁹ In addition, we summarized the electrocatalytic activity of MPEA materials synthesized using various approaches for the acidic HER reaction (Table S5†). It is evident that the MPEA catalysts synthesized *via* the co-reduction method exhibit superior HER performance while offering a facile synthesis process.

Conclusions

In summary, MPEA nanocatalysts, including RuPt/C, RuPtIr/C, RuPtIrSn/C, and RuPtIrSnCu/C with ultrafine sizes ($\sim 3.0 \text{ nm}$) and high dispersion were synthesized using a rapid co-reduction strategy without employing surfactants. This method allows for the precise tuning of the composition of nanoalloys, enabling the MPEAs with arbitrary combinations of Ir, Sn, and Cu elements along with Ru and Pt. Structural characterization including XRD and AC-TEM confirmed the FCC structure of these MPEA nanoparticles with no phase separation within the particles. Electrochemical experiments revealed that RuPtIrSnCu/C exhibits the best HER activity and stability among the as-synthesized MPEA catalysts, attributed to the enhanced synergetic and high entropy effects that are magnified with the increasing number of components. The proposed rapid co-reduction synthesis method facilitates the efficient production of MPEA nanomaterials without requiring complex experimental facilities. Moreover, its surfactant-free nature imparts promising catalytic potential to the as-synthesized MPEA catalysts.

Data availability

The data that support the findings of this study are available from the corresponding author upon reasonable request.

Conflicts of interest

There are no conflicts to declare.

Acknowledgements

This work was financially supported by the National Natural Science Foundation of China (22376062 and 22109043), the

Science and Technology Commission of Shanghai Municipality (22ZR1415700), and the Fundamental Research Funds for the Central Universities.

References

- 1 J. W. Yeh, S. K. Chen, S. J. Lin, J. Y. Gan, T. S. Chin, T. T. Shun, C. H. Tsau and S. Y. Chang, *Adv. Eng. Mater.*, 2004, **6**, 299–303.
- 2 Y. Zhang, *Prog. Mater. Sci.*, 2014, **61**, 1–93.
- 3 P.-Y. Cao, F. Liu, F.-P. Yuan, E. Ma and X.-L. Wu, *Mater. Today Nano*, 2024, **28**, 100511.
- 4 G. Han, M. Li, H. Liu, W. Zhang, L. He, F. Tian, Y. Liu, Y. Yu, W. Yang and S. Guo, *Adv. Mater.*, 2022, **34**, 2202943.
- 5 X. Zhang, C. Cao, T. Ling, C. Ye, J. Lu and J. Shan, *Adv. Energy Mater.*, 2024, 2402633.
- 6 Y. Yang, C. Hu, J. Shan, C. Cheng, L. Han, X. Li, R. Wang, W. Xie, Y. Zheng and T. Ling, *Angew. Chem., Int. Ed.*, 2023, **62**, e202300989.
- 7 J. Guo, R. Wang, Q. Wang, R. Ma, J. Li, E. Zhao, J. Shan and T. Ling, *Nano Res.*, 2024, **17**, 9483–9489.
- 8 M. Liu, Z. Zhang, F. Okejiri, S. Yang, S. Zhou and S. Dai, *Adv. Mater. Interfaces*, 2019, **6**, 1900015.
- 9 T. Jin, X. Sang, R. R. Unocic, R. T. Kinch, X. Liu, J. Hu, H. Liu and S. Dai, *Adv. Mater.*, 2018, **30**, 1707512.
- 10 Y. Xin, S. Li, Y. Qian, W. Zhu, H. Yuan, P. Jiang, R. Guo and L. Wang, *ACS Catal.*, 2020, **10**, 11280–11306.
- 11 T. Löffler, A. Savan, A. Garzón-Manjón, M. Meisch, C. Scheu, A. Ludwig and W. Schuhmann, *ACS Energy Lett.*, 2019, **4**, 1206–1214.
- 12 Y. Yao, Z. Huang, P. Xie, S. D. Lacey, R. J. Jacob, H. Xie, F. Chen, A. Nie, T. Pu, M. Rehwoldt, D. Yu, M. R. Zachariah, C. Wang, R. Shahbazian-Yassar, J. Li and L. Hu, *Science*, 2018, **359**, 1489–1494.
- 13 F. Waag, Y. Li, A. R. Zieffuß, E. Bertin, M. Kamp, V. Duppel, G. Marzun, L. Kienle, S. Barcikowski and B. Gökce, *RSC Adv.*, 2019, **9**, 18547–18558.
- 14 B. Wang, C. Wang, X. Yu, Y. Cao, L. Gao, C. Wu, Y. Yao, Z. Lin and Z. Zou, *Nat. Synth*, 2022, **1**, 138–146.
- 15 T. Löffler, H. Meyer, A. Savan, P. Wilde, A. Garzón Manjón, Y.-T. Chen, E. Ventosa, C. Scheu, A. Ludwig and W. Schuhmann, *Adv. Energy Mater.*, 2018, **8**, 1802269.
- 16 S. Gao, S. Hao, Z. Huang, Y. Yuan, S. Han, L. Lei, X. Zhang, R. Shahbazian-Yassar and J. Lu, *Nat. Commun.*, 2016, **2020**, 11.
- 17 G. R. Dey, C. R. McCormick, S. S. Soliman, A. J. Darling and R. E. Schaak, *ACS Nano*, 2023, **17**, 5943–5955.
- 18 X. Mou, X. Wei, Y. Li and W. Shen, *CrystEngComm*, 2012, **14**, 5107–5120.
- 19 H.-Q. Wu, X.-W. Wei, M.-W. Shao, J.-S. Gu and M.-Z. Qu, *J. Mater. Chem.*, 2002, **12**, 1919–1921.
- 20 H. Wang, W. Luo, L. Zhu, Z. Zhao, B. E. W. Tu, X. Ke, M. Sui, C. Chen, Q. Chen, Y. Li and Y. Huang, *Adv. Funct. Mater.*, 2018, **28**, 1707219.
- 21 S. K. Nemani, R. K. Annavarapu, B. Mohammadian, A. Raiyan, J. Heil, M. A. Haque, A. Abdelaal and H. Sojoudi, *Adv. Mater. Interfaces*, 2018, **5**, 1801247.
- 22 Y. Sun and S. Dai, *Sci. Adv.*, 2021, **7**, eabg1600.
- 23 Q. Zhang, K. Lian, Q. Liu, G. Qi, S. Zhang, J. Luo and X. Liu, *J. Colloid Interface Sci.*, 2023, **646**, 844–854.
- 24 H.-J. Song, X.-H. Jia, X.-F. Yang, H. Tang, Y. Li and Y.-T. Su, *CrystEngComm*, 2012, **14**, 405–410.
- 25 D. Wu, K. Kusada, T. Yamamoto, T. Toriyama, S. Matsumura, I. Gueye, O. Seo, J. Kim, S. Hiroi, O. Sakata, S. Kawaguchi, Y. Kubota and H. Kitagawa, *Chem. Sci.*, 2020, **11**, 12731–12736.
- 26 G. Feng, F. Ning, J. Song, H. Shang, K. Zhang, Z. Ding, P. Gao, W. Chu and D. Xia, *J. Am. Chem. Soc.*, 2021, **143**, 17117–17127.
- 27 Z.-T. Yan, S. Tao, J. Wang, X.-L. Lu and T.-B. Lu, *Adv. Mater.*, 2024, 2411942.
- 28 Y. Wan, W. Wei, S. Ding, L. Wu, H. Qin and X. Yuan, *Adv. Funct. Mater.*, 2024, 2414554.
- 29 J.-W. Yeh, *JOM*, 2013, **65**, 1759–1771.